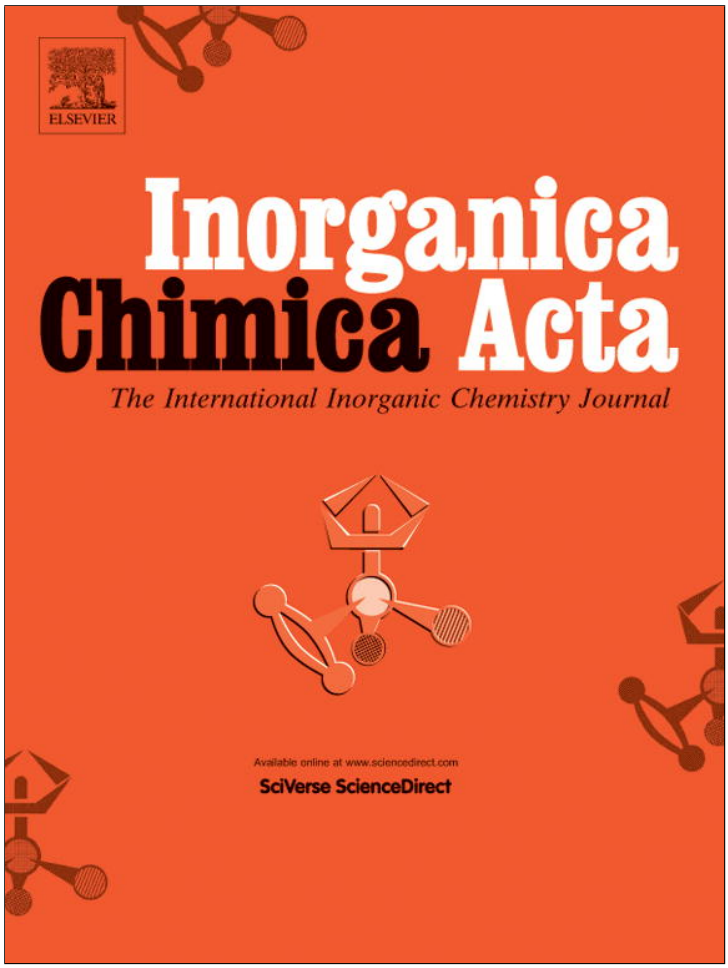

Inorganica Chimica Acta 405 (2013) 362–367

Contents lists available at SciVerse ScienceDirect

Inorganica Chimica Acta

journal homepage: www.elsevier.com/locate/ica

Synthesis of two novel dinuclear molybdenum(0) complexes of quinoxaline-2,3-dione: New precursors for preparation of α-MoO_3 nanoplates

Mostafa Y. Nassar [a,*], Attia S. Attia [b], Khalifa A. Alfallous [b], M.F. El-Shahat [b,*]

[a] Chemistry Department, Faculty of Science, Benha University, Benha 13518, Egypt
[b] Chemistry Department, Faculty of Science, Ain Shams University, Abbasia, Cairo 11566, Egypt

ARTICLE INFO

Article history:
Received 1 May 2013
Received in revised form 18 June 2013
Accepted 18 June 2013
Available online 26 June 2013

Keywords:
Chemical synthesis
X-ray diffraction
Optical properties
Organometallic compounds
Nanostructures

ABSTRACT

α-MoO_3 nanoplates have been prepared through thermal decomposition of two novel organometallic molybdenum complexes, as new solid precursors, at 500 °C for 2 h. The two molybdenum complexes ($[(Mo_2(bipy)(CO)_n(DQ)_m]$; where, DQ = quinoxaline-2,3-dione; $n = 2$ or 4, $m = 2$ or 3) were synthesized by reaction of $Mo(CO)_6$, and DQ in presence of 2,2′-bipyridine in THF solvent at reflux temperature under atmospheric or reduced pressure. Interestingly, the crystallite size of the produced MoO_3 nanoplates products (80.7 and 114 nm) depended on the organic moiety content of the ignited solid precursor. The as-prepared products were characterized by means of elemental analysis, Fourier transform infrared spectroscopy (FT-IR), UV–Vis spectroscopy, thermal analysis (TGA), X-ray powder diffraction (XRD), Field emission electron microscopy (FESEM) and mass spectroscopy. The produced MoO_3 nanoplates showed semiconducting properties by exhibiting optical band gab energy of 3.0 or 3.25 eV.

1. Introduction

Molybdenum trioxide (MoO_3) is well known as one of the most important transition metal oxides due not only to its rich chemistry associated with multiple valence states but also to its high chemical and thermal stability. It exists mainly in three polymorphs called orthorhombic α-MoO_3, monoclinic β-MoO_3, and hexagonal γ-MoO_3 [1,2]. Generally, nano-sized MoO_3 is still an attractive material for its unusual physical and chemical properties, and its wide application. Due to its unique structural and optical properties, molybdenum trioxide is a promising material for various industrial applications such as catalysis, sensors, photochromic and electro-chromic devices, display materials, and battery systems [3–7]. Also, it was used as a good precursor for synthesizing various other important materials, such as $MoSe_2$, MoS_2, Mo and host–guest compounds [8–11]. Despite the importance of MoO_3 nanomaterial, successful synthesis of such structures is still limited. Various techniques such as thermal evaporation under vacuum conditions [12], hydrothermal method [13], chemical route [14], and sol–gel method [15] have been developed to explore novel architectures and morphologies of this important nanosized material. Although, these methods are successful in synthesis of MoO_3 nanomaterials, many of them need either vacuum or low-pressure conditions, and the chemical and hydrothermal methods are not only complicated but also more or less produce contamination.

On the other hand, using coordination or organometallic compounds as new precursors to produce metal oxide nanoparticles has recently received much attention and has been explored as an efficient route for this purpose [16–19]. This methodology involves the thermal decomposition of a metallo-organic compound, leading to the formation of the metal oxide of interest. From the practical point of view, this route does not require an inert atmosphere, vacuum, or a sophisticated apparatus when compared with the other aforementioned techniques.

In our group, we have been interested in synthesis of metal oxide nanoparticles [20–22]. A major interest at the moment is using new metallo-organic compounds as precursors for preparation of metal oxide nanoparticles to control nanocrystal size, distribution size, and also morphology. Additionally, although the quinoxaline derivatives are very important and readily available ligands, to the best of our knowledge, 1,4-dihydro-quinoxaline-2,3-dione molybdenum complexes have not been used as solid precursors to produce MoO_3 nanoparticles through their thermal decomposition.

Herein, we reported, for the first time, the synthesis of two novel quinoxaline-2,3-dione bimolybdenum complexes. The as-prepared organometallic complexes were then used as solid precursors to produce pure α-MoO_3 nanoplates by thermal decomposition at 500 °C for 2 h. The as-prepared products were

* Corresponding authors. Tel.: +20 1068727555 (M.Y. Nassar), tel.: +20 1128323115 (M.F. El-Shahat).
E-mail addresses: m_y_nassar@yahoo.com (M.Y. Nassar), elshahatmf@hotmail.com (M.F. El-Shahat).

0020-1693/$ - see front matter © 2013 Elsevier B.V. All rights reserved.
http://dx.doi.org/10.1016/j.ica.2013.06.030

characterized using XRD, TGA analyses, mass spectra, FESEM, FT-IR, and UV–Vis spectra. Plus, the optical properties of the produced molybdenum oxide nanoparticles were investigated.

2. Experimental

2.1. Materials and reagents

Molybdenum hexacarbonyl, $Mo(CO)_6$, 2,2′-bipyridine, bipy, oxalic acid,$C_2H_2O_4{\cdot}2H_2O$, and 1,2-phenylenediamine, $C_6H_8N_2$, were used as purchased from Sigma–Aldrich Chemical Co. Inc. quinoxaline-2,3-dione (DQ) ligand was synthesized according to the reported literature [23]. All solvents were of analytical reagent grade and purified according to the standard methods [24].

2.2. Synthesis of precursors

2.2.1. Synthesis of $[Mo_2(bipy)(CO)_4(DQ)_2]$ complex (**A**)

$Mo(CO)_6$ (0.150 g, 0.568 mmol) and bipyridine (0.089 g, 0.570 mmol) were mixed in 20 mL of THF, stirred and refluxed under nitrogen gas for 30 min. The obtained light red colored solution was allowed to cool down to room temperature, and a THF solution (10 mL) of DQ (0.092 g, 0.570 mmol) was then added drop wise. The reaction blend was then refluxed again at atmospheric pressure for 11 h, during which the reaction mixture turned into reddish brown color. The solid product was collected by filtration and washed with THF, hot petroleum ether, and diethyl ether and then dried under vacuum. A slow diffusion of THF solvent into a concentrated DMF solution of the crude solid produced reddish brown microcrystals of the product which were then collected by filtration and dried under vacuum to give a pure reddish-brown product (0.17 g, 76.3%). *Anal.* Calc. For $C_{30}H_{20}Mo_2N_6O_8$ (MW = 784.40): C, 45.94; H, 2.57; N, 10.71%. Found: C, 45.59; H, 2.22; N, 10.80%. EI-MS: *m*/*z* 749 [M−($2H_2O$+$3H^+$)], 695 [M−(2CO+$2H_2O$)], 631 [M−(bipyridine)]. ^{1}H NMR (DMSO-d_6), δ, ppm: 7.12 (d, 8H, 2DQ), 11.91 (s, 4H, 2DQ), δ 7.6 (t, 2H, bypyridine), 8.17 (t, 2H, bypyridine), 8.6 (d, 2H, bypyridine), 8.9 (d, 2H, bypyridine).

2.2.2. Synthesis $[Mo_2(bipy)(CO)_2(DQ)_3]$ complex (**B**)

$Mo(CO)_6$ (0.150 g, 0.568 mmol) and bipyridine (0.089 g, 0.570 mmol), and 30 mL THF were stirred together and heated at reflux for 30 min, during which color of the reaction mixture turned into light red. The reaction blend was then allowed to get the room temperature (25 °C), and a THF solution (15 mL) of DQ (0.092 g, 0.570 mmol) was then added drop wise. The reaction mixture was heated to reflux temperature under reduced pressure in a Schlenk tube for 15 h, during which color of the reaction blend changed into a reddish orange. The solid material was isolated by filtration then washed several times with THF, hot petroleum ether, and then with diethyl ether. The crude product was crystallized by slow diffusion of THF solvent into DMF solution of the product to give reddish orange microcrystals of the complex. The microcrystals were collected by filtration and dried under vacuum to give 0.158 g of the desired product (62.2% yield). *Anal.* Calc. For $C_{36}H_{26}Mo_2N_8O_8$ (MW = 890.52): C, 48.55; H, 2.94; N, 12.58%. Found: C, 48.34; H, 2.76; N, 12.29%. EI-MS: *m*/*z* 838 [M−(2CO+H_2-O)], 695 [M−(DQ+bipyridine)]. ^{1}H NMR (DMSO-d_6), δ, ppm: 7.10 (d, 12H, 3DQ), 11.90 (s, 6H, 3DQ), δ 7.64 (t, 2H, bypyridine), 8.19 (t, 2H, bypyridine), 8.82 (d, 2H, bypyridine), 9.05 (d, 2H, bypyridine).

2.3. Preparation of nano-sized molybdenum trioxide (MoO_3)

The as–prepared molybdenum complex precursors (**A** and **B**) were thermally decomposed for two hours at 500 °C in an open air electric furnace to produced nano-sized molybdenum trioxides; A-MoO_3, and B-MoO_3, respectively.

2.4. Physical measurements

Elemental analysis was performed using a Perkin-Elmer 2400 CHN elemental analyzer. The infrared spectra (4000–400 cm^{-1}) were recorded as KBr pellets on a Perkin Elmer 550 FTIR spectrometer. The ^{1}H NMR spectra were recorded using 300 MHz Varian-Oxford Mercury. The thermal behavior of the samples was studied with thermal analysis techniques. Thermogravimetric (TGA 7, Shimadzu DT-30) measurements were performed with heating rate 10 °C/min, under nitrogen atmosphere. The EI mass spectra were recorded by the EI technique at 70 eV with a Schimadzu-GCMSQP 1000EX quadruple mass spectrometer with electron multiplier detector equipped with a GC–MS data system. The structures and phase compositions of the as-synthesized MoO_3 products were characterized by powder X-ray diffraction (XRD) using an 18 KW automated diffractometer (Bruker; model D8 advance) with monochromatic Cu Kα radiation (λ 1.54178 Å). FESEM images were taken using field emission scanning electron microscope (FESEM) with a microscope (JEOL JSM-6500F). UV–Vis. spectra were recorded on Jasco; model v530.

3. Results and discussion

3.1. Synthesis and characterization of the Mo-organometallic precursors

The precursor complexes (**A** and **B**) were prepared by the reaction of $Mo(CO)_6$ with quinoxaline-2,3-dione in THF in 1:1 ratio under refluxing. However, complex **A** was prepared under atmospheric pressure but complex **B** was prepared under a reduced pressure in a Schlenk tube. Characterization of the complexes was carried out by IR, ^{1}H NMR, elemental analysis, thermal analysis, and mass spectra. The structures of the complexes are shown in Scheme 1.

3.1.1. Infrared study

In the IR spectra, the free DQ ligand exhibited characteristic frequencies at ~3150, 1712, 1480, and 1400 cm^{-1} which can be assigned to ν(NH), ν(C=O), and $\nu(CN)_{amide}$, and δ(NH), respectively [23,25]. This spectral behavior is in good agreement with the solid-state structure of the ligand. The IR spectrum of the complex **A** showed new bands at 2008.7 and 1915.6 cm^{-1} which can be attributed to a terminal coordinated CO and new bands at 1869.6 and 1815.4 cm^{-1} which can be assigned to bridged CO groups which are consistent with the published data [26–28]. On the other hand, interestingly, the IR spectrum of complex **B** revealed presence of characteristic frequencies at 1870.3 and 1816.1 cm^{-1} which are due to bridged CO groups only. However, the C=O frequency of the free ligands was shifted to lower frequency region

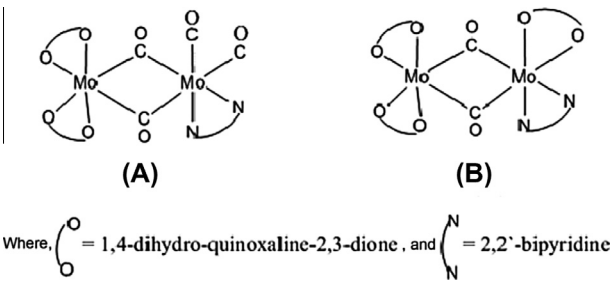

Scheme 1. Proposed structures for the as-prepared molybdenum complexes (**A** and **B**).

in the complexes and appeared at 1700 and 1695 cm^{-1}, for **A** and **B** complexes, respectively. Additionally, the presence of a band at around 550 cm^{-1} assigned to ν(M–O) for both complexes supports the proposed mode of coordination[29]. The spectra of the complexes also exhibited absorption band at around 1560 cm^{-1} which could be assigned to coordinated C=N functional groups of the bipyridine ligand that in turn was also confirmed by presence of a weak absorption band at around 420 cm^{-1} which could be assigned to ν(M–N), supporting the coordination mode of the two complexes presented in Scheme 1.

3.1.2. Proton NMR study

The diamagnetism of the isolated molybdenum complexes has further been confirmed from their ^{1}H NMR spectral measurements. The ^{1}H NMR spectra of the DQ ligand and its complexes have been recorded in DMSO-d_6. The DQ ligand showed one doublet at δ7.05 ppm with four protons assigned to the aromatic protons of the ligand, and one singlet at 11.87 ppm with two protons assigned to the NH of the ligand, which both signals are in agreement with the ligand's composition. However, on reaction with $Mo(CO)_6$, position of these signals has not been shifted too much and the aromatic protons of the coordinated DQ ligand appeared as a doublet signal at δ7.12 (8 H), and 7.10 (12 H) ppm for complex **A** and **B**, respectively. The complexes **A** and **B** exhibited a singlet at 11.91 (4 H), and 11.90 (6 H) ppm, respectively, which might be attributed to NH of the coordinated DQ ligand. From the integration of the DQ proton-signal for both complexes, it could be concluded that there are two and three coordinated DQ ligands for complexes **A** and **B**, respectively. Interestingly, the ^{1}H NMR spectrum of complex **A** also showed signals at δ 7.6 (t, 2H, bypyridine), 8.17 (t, 2H, bypyridine), 8.6 (d, 2H, bypyridine), and 8.9 (d, 2H, bypyridine) ppm which can be assigned to a coordinated bypyridine molecule. On the other hand, ^{1}H NMR spectrum of **B** complex showed signals at δ 7.64 (t, 2H, bypyridine), 8.19 (t, 2H, bypyridine), 8.82 (d, 2H, bypyridine), and 9.05 (d, 2H, bypyridine) ppm which can be assigned to one coordinated bypyridine molecule.

3.1.3. Thermal analysis

The thermal analyses (TGA) curves of the as-prepared precursor complexes (**A** and **B**) carried out within a temperature range from room temperature to 1000 °C are shown in Fig. 1. The thermal decomposition of the A-complex, $[Mo_2(bipy)(CO)_4(DQ)_2]$, as shown in Fig. 2a, reveals presence of four mass loss steps. The first step in the temperature range 107–227 °C can be attributed to the loss of bipyridine ligand with a weight loss of 20.38% (calc. 20.0%). The second significant weight loss observed from 227 to 372 °C corresponding to the decomposition of one molecule of the DQ ligand and four molecules of CO, 33.45% (calc. 34.9%). This is followed by decomposition of the second DQ-ligand molecule in the temperature range 374–587 °C, 19.3% (calc. 20.6%), with a residue amounting to Mo_2O and carbon, 26.5% (calc. 24.50% for Mo_2O) which upon increasing the temperature, at the current thermal analysis conditions, Mo_2O can be converted into MoO_3 at 679 °C which subsequently may undergo slow sublimation on increasing the temperature. On the other hand, Fig. 1b depicts the thermogram of the complex (**B**). Four stages of weight loss have been observed. The weight loss in the temperature range 113–200 °C can be ascribed to the loss of bipyridine ligand and one molecule of CO, 20.05% (calc. 20.68%). The second stage weight loss in the temperature 200–385 °C can be attributed to decomposition of two molecules of the DQ-ligand and one molecule of CO with total mass loss of 39.20% (calc. 39.56%). The last molecule of the DQ-ligand was decomposed in the temperature range 387–480 °C, with a weight loss of 17.60% (calc 18.20%) leaving Mo_2O and carbon residues with 21.56% and 1.59%, respectively. Finally, Mo_2O was converted under the thermal analysis conditions into MoO_3 upon increasing the temperature above 746 °C which subsequently underwent slow sublimation. Finally, the thermal decomposition steps of the complexes (**A** and **B**) are formulated in Scheme 2.

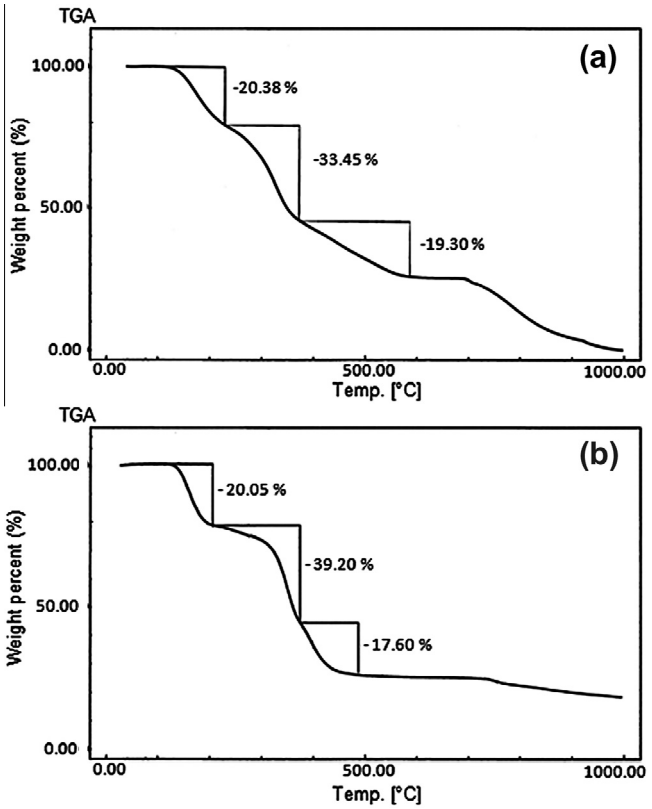

Fig. 1. (a, b) Thermal analysis of the as-prepared molybdenum complexes (**A** and **B**) in nitrogen atmosphere.

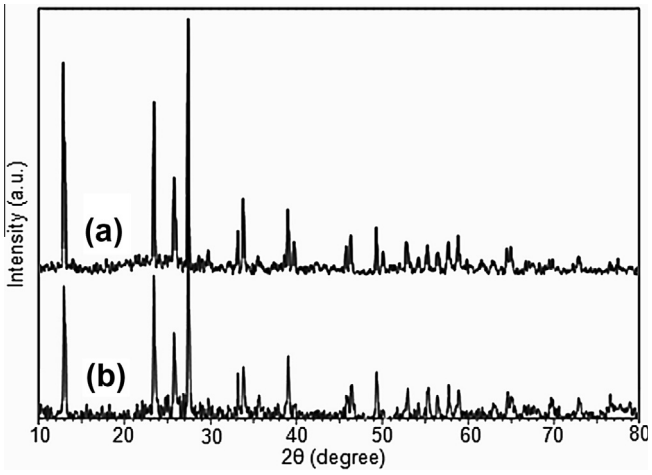

Fig. 2. (a, b) XRD patterns of the A-MoO_3 and B-MoO_3 nanoplates produced by thermal decomposition of **A** and **B** complexes, respectively.

3.1.4. Mass spectroscopy

The as-prepared complexes were further characterized using mass spectroscopy. The mass spectrum of complex **A** exhibited fragments at m/z = 749, 695, 631, 298, 220, and 162 which may be attributed to M–($2H_2O$+$3H^+$), M–(2CO+$2H_2O$), M–(bipyridine), (M-(bipyridine))/2–H_2O, (M/2)–(bipyridine+H_2O), and DQ, respectively. On the other hand mass spectrum of complex **B** revealed

- Thermal decomposition of complex (A):

1- $[Mo_2(bipy)(CO)_4(DQ)_2]$ —(107 - 227 °C; -bipy; -20.38 %)→ $[Mo_2(CO)_4(DQ)_2]$

2- $[Mo_2(CO)_4(DQ)_2]$ —(227 - 372 °C; (-DQ, - 4 CO); - 33.45 %)→ $[Mo_2(DQ)]$

3- $[Mo_2(DQ)]$ —(374 - 587 °C, TGA conditions; - DQ; -19.3 %)→ Mo_2O + carbon residue

4- Mo_2O —(> 679 °C; under TGA conditions)→ MoO_3

- Thermal decomposition of complex (B):

1- $[Mo_2(bipy)(CO)_2(DQ)_3]$ —(113 - 200 °C; (-bipy, -CO); -20.05 %)→ $[Mo_2(CO)(DQ)_3]$

2- $[Mo_2(CO)(DQ)_3]$ —(200 - 385 °C; (-2DQ, - CO); - 39.20 %)→ $[Mo_2(DQ)]$

3- $[Mo_2(DQ)]$ —(387 - 480 °C, TGA conditions; - DQ; -17.60 %)→ Mo_2O + carbon residue

4- Mo_2O —(> 746 °C; under TGA conditions)→ MoO_3

Scheme 2. The proposed thermal decomposition of **A** and **B** complexes.

fragments at $m/z = 838$, 576, and 156 which may correspond to M–(2CO+H_2O), M–(DQ+bipyridine), and $HMoO_2CN$, respectively. All the previously mentioned analytical spectroscopic results could confirm and verify the proposed structures of the as-prepared precursor complexes (**A** and **B**), Scheme 1.

3.2. MoO_3 nanoplates

3.2.1. Preparation, morphology and spectral characterization

XRD patterns of the molybdenum trioxide nanoplates produced by thermal decomposition of the as-prepared solid precursors; **A** and **B** complexes, at 500 °C for 2 h, respectively, are shown in Fig. 2. It is clearly observed that all the reflections can be indexed to a pure crystalline orthorhombic α-MoO3 phase (JCPDS card No. 05-0508, S.G. *Pbnm*, $a = 3.962$ Å, $b = 13.858$ Å, and $c = 3.697$ Å). Peaks due to other phases are not identified in the samples, indicating high purity of the as prepared α-MoO_3 nanoplates. The crystallite size (D, nm) of the α-MoO_3 samples are calculated using the Scherrer Eq. (1)[30].

$$D = 0.89\lambda/\beta\cos\theta_B \quad (1)$$

Where λ, β, θ_B are the X-ray wavelength, the full width at half maximum (FWHM) of the diffraction peak and the Bragg diffraction angle respectively. The estimated average crystallite size of MoO_3 nanoplates was found to be *ca.* 114 and 80.7 nm, for A-MoO_3, and B-MoO_3, respectively. According to the obtained crystallite size of the produced oxides, and the prepared complexes (**A** and **B**) which have metal-to-ligand (Mo/DQ) ratio equals to 1:1 and 1:0.67, respectively, it can be concluded that the crystallite size of the produced MoO_3 nanoplates depends on how many ligands each complex has. It is clearly seen that by increasing DQ molecules around the Mo metal, MoO_3 nanoparticles with smaller crystallite size could be obtained and this might be attributed to that when metal-to-ligand ratio equals to 1:0.67, Mo atoms may be almost capped completely with DQ ligands, and in turn the Mo atoms might be protected against agglomeration during the ignition process [31]. Fig. 3 shows FT-IR spectra for the orthorhombic (α)-MoO_3 products. It exhibits sharp peak at 992.7 and 993.4 cm^{-1}, for A-MoO_3, and B-MoO_3, respectively. Also, it reveals broad and strong peak at 871.6 and 865.5 cm^{-1} for A-MoO_3, and B-MoO_3, respectively. There is another broad peak at 585.6 and 561.2 cm^{-1} for A-MoO_3, and B-MoO_3, respectively, corresponding to interaction of oxygen atom with three metal atoms (O-3Mo) and these peaks are consistent with the published data for orthorhombic MoO_3[32]. However, the IR spectra of the A-MoO_3, and B-MoO_3 products show absorptions at (3453 and 1631 cm^{-1}) and at (3303, 3530 and 1630) cm^{-1}, respectively, which can be assigned to the stretching and bending vibrations of the adsorbed surface molecular water interacting with MoO_3 products and the broadness of these bands can be attributed to hydrogen-bonding O–H [29].

The morphology of the as-prepared α-MoO_3 nanostructures was investigated using field emission scanning microscopy (FE-SEM), and the images are presented in Fig. 4. Fig. 4(Ia) shows a low magnification the FE-SEM image for the as-prepared A-MoO_3 and this image exhibits assemblies of irregular plates. However, the magnified FE-SEM image (Fig. 4(Ib)) shows that the assemblies of A-MoO_3 product is made of square like and rectangular like plates with an average length of less than 1.5 and 15 μm, respectively, and with a width of 1.5 and 2.5 μm, respectively. Also, most of these plates are actually multilayer plates with a thickness of less than 2 μm. Some of these plates have smooth surface and the other do not. On the other hand, a lower magnification FE-SEM image, Fig. 4(IIa), shows the overview of plate assemblies for B-MoO_3, and these assemblies are composed of square like, hexagonal like and truncated hexagonal like plates. Detailed inspection of a single assembly at higher magnification is shown in Fig. 4(IIb), which reveals that these plates have smooth surface and are fairly uniform with an average length of less than 10 μm, a width of ca. 1 μm, and a thickness of ca. 400 nm.

3.2.2. Optical properties of MoO_3 nanoplates

Optical properties: The UV absorption spectra of the as-prepared molybdenum trioxide samples obtained from different precursors were taken and, subsequently, the optical band gap (E_g) of the as-prepared nanosized MoO_3 can be calculated using the Tauc's relation (Eq. (2)) [33,34]:

$$(\alpha h\nu) = K(h\nu - E_g)^n \quad (2)$$

where K is a parameter that depends on the transition probability and involves properties of the bands, $h\nu$ is the photon energy, E_g is the optical band gap, and n is ½, 3/2, 2, or 3 for transitions which are directly allowed, directly forbidden, indirectly allowed, or indirectly forbidden, respectively [35]. Fig. 5 shows the absorption coefficient in the form of $(\alpha h\nu)^2$ plotted versus $h\nu$ values for the MoO_3 nanoplates. The extrapolation of each graph to $(\alpha h\nu)^2 = 0$ yields the optical direct band gap (E_g) which was found to be 3.01 and

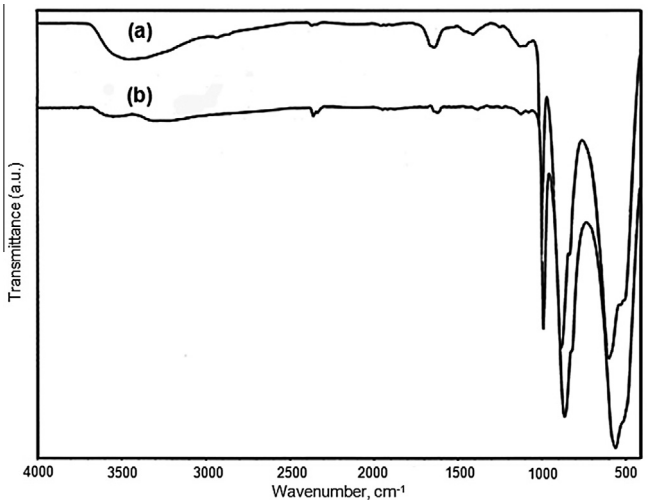

Fig. 3. (a, b) FT-IR spectrum of the produced A-MoO_3 and B-MoO_3 nanoplates after calcinations at 500 °C in air for 2 h.

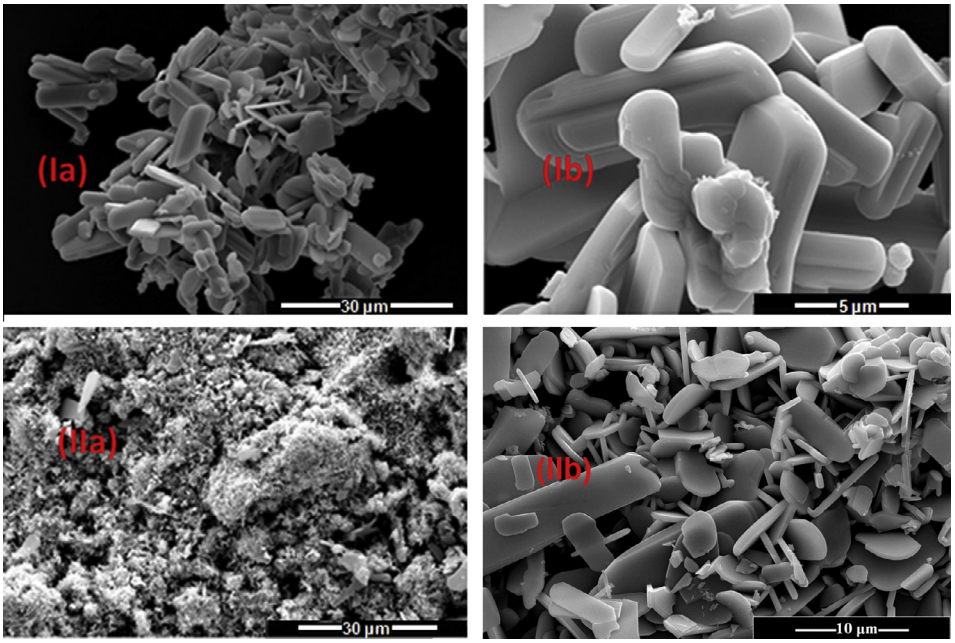

Fig. 4. (I, II) SEM images (low (a) and high (b) magnification) of the as produced A-MoO3 and B-MoO3 nanoplates, respectively.

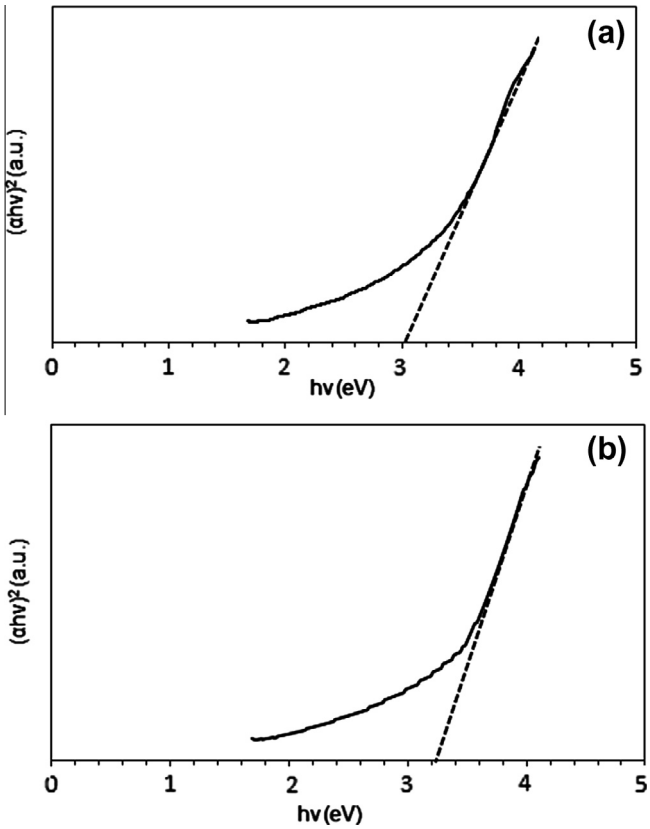

Fig. 5. (a, b) $(\alpha h\nu)^2 \sim h\nu$ curves; a and b, for the prepared A-MoO_3 and B-MoO_3 samples, respectively.

3.25 eV for A-MoO_3 and B-MoO_3 nanoplates respectively. These values mean that the energy band gaps of the as-prepared nano-sized MoO_3 products are inverse proportional to their crystallite sizes. These values reveal that the as-prepared molybdenum trioxide nanoplates products are semiconductors. These values are in good agreement with the reported data [33,36].

4. Conclusion

α-MoO_3 nanoplates were synthesized via thermal decomposition of two new molybdenum complexes, as solid precursors. The two novel molybdenum complexes were synthesized by reaction of $Mo(CO)_6$, and quinoxaline-2,3-dione (DQ) ligand in presence of 2,2′-bipyridine at reflux temperature. Increasing the ligand to metal ratio in the synthesized complex resulted in smaller crystallite size of the produced MoO_3 nanomaterials. The crystallite size was found to be 114 and 82 nm for MoO_3 produced from [Mo_2(bipy)$(CO)_4(DQ)_2$], and [Mo_2(bipy)$(CO)_2(DQ)_3$], solid precursors, respectively. The optical energy gap was also controlled by controlling the crystallite size and it was found that MoO_3 with larger crystallite size has smaller energy gap (3.0 eV) and that with smaller crystallite size has bigger energy gap (3.25 eV). The as-prepared products were characterized by FT-IR, UV–Vis, Mass, FESEM, thermal analysis, and XRD spectroscopy.

References

[1] X.W. Lou, H.C. Zeng, Chem. Mater. 14 (2002) 4781.
[2] Z. Wang, S. Madhavi, J. Phys. Chem. C 116 (2012) 12508.
[3] W. Li, F. Cheng, Z. Tao, J. Chen, J. Phys. Chem. B 110 (2006) 119.
[4] A.M. Taurino, A. Forleo, L. Francioso, P. Siciliano, Appl. Phys. Lett. 88 (2006) 152111 (3 pp).
[5] S. Hamwi, J. Meyer, T. Winkler, T. Riedl, W. Kowalsky, Appl. Phys. Lett. 94 (2009) 253307. 3 pp.
[6] B. Yen, Z. Zheng, J. Zhang, H. Gong, Z. Shan, W. Huang, T. Yu, J. Phys. Chem. C113 (2009) 20259.
[7] D. Mariotti, H. Lindstrom, A.C. Bose, K. Ostrikov, Nanotechnology 19 (2008) 495302 (6 pp).
[8] L. Margulils, G. Salitra, R. Tenne, M. Talianker, Nature (Lond.) 365 (1993) 113.
[9] Y. Feldman, E. Wasserman, D.J. Srolovitz, R. Tenne, Science 267 (1995) 222.
[10] P.J. Hagrman, D. Hagrman, J. Zubieta, Angew. Chem., Int. Ed. Engl. 38 (1999) 2638.
[11] M. Hershfinkel, L.A. Gheber, V. Volterra, J.L. Hutchison, L. Margulis, R. Tenne, J. Am. Chem. Soc. 116 (1994) 1914.
[12] X.F. Duan, C.M. Lieber, Adv. Mater. 12 (2000) 298.
[13] R.Q. Song, A.W. Xu, B. Deng, Y.P. Fang, J. Phys. Chem. B 109 (2005) 22758.
[14] G.C. Li, L. Jiang, S.P. Pang, H.G. Peng, Z.K. Zhang, J. Phys. Chem. B 110 (2006) 24472.
[15] G. Wang, Y. Ji, L. Zhang, Y. Zhu, P.I. Gouma, M. Dudley, Chem. Mater. 19 (2007) 979.
[16] E. de B. Santos, F.A. Sigoli, I.O. Mazali, J. Solid State Chem. 190 (2012) 80.

[17] I.O. Mazali, B.C. Viana, O.L. Alves, J.M. Filho, A.G.S. Filho, J. Phys. Chem. Solids 68 (2007) 622.
[18] D. Cangussu, W.C. Nunes, H.L.S. Corrêa, W.A.A. Macedo, M. Knobel, O.L. Alves, A.G.S. Filho, I.O. Mazali, J. Appl. Phys. 105 (2009) 013901 (7 pp).
[19] C.M. Ronconi, D. Gonçalves, N. Suvorova, O.L. Alves, E.A. Irene, J. Phys. Chem. Solids 70 (2009) 234.
[20] M.Y. Nassar, Mater. Lett. 94 (2013) 112.
[21] M.Y. Nassar, I.S. Ahmed, Polyhedron 30 (2011) 2431.
[22] M.Y. Nassar, I.S. Ahmed, Mater. Res. Bull. 47 (2012) 2638.
[23] H. Thakuria, G. Das, J. Chem. Sci. 118 (2006) 425.
[24] W.L.F Armarego, D.D. Perrin, Purification of Laboratory Chemicals, fourth ed., Butterworth-Heinemann, Oxford, U.K., 2000.
[25] K.F. Konidaris, G.S. Papaefstathiou, G. Aromi, S.J. Teat, E. Manessi-Zoupa, A. Escuer, S.P. Perlepes, Polyhedron 28 (2009) 1646.
[26] M.D. Randles, V. Gupta, P.V. Simpson, G.J. Moxey, A.L. Criddle, R. Stranger, M.P. Cifuentes, M.G. Humphrey, Polyhedron 52 (2013) 957.
[27] B. Li, B. Wang, S. Xu, X. Zhou, J. Organomet. Chem. 690 (2005) 5309.
[28] T. Munisamy, S.L. Gipson, A. Franken, Inorg. Chim. Acta 363 (2010) 20.
[29] K. Nakamoto, Infrared and Raman Spectra of Inorganic and Coordination Compounds. Part B: Applications in Coordination, Organometallic, and Bioinorganic Chemistry, sixth ed., Wiley-Interscience, USA, 2009.
[30] R. Jenkins, R.L. Snyder, Chemical Analysis: Introduction to X-ray Powder Diffractometry, John Wiley and Sons, Inc., New York, 1996.
[31] M. Salavati-Niasari, F. Mohandes, F. Davar, M. Mazaheri, M. Monemzadeh, N. Yavarinia, Inorg. Chim. Acta 362 (2009) 3691.
[32] A. Chithambararaj, A.C. Bose, J. Alloys Compd. 509 (2011) 8105.
[33] M.P. Dare-Edwards, A.H. Goodenough, A. Hammett, P.R. Trevellick, J. Chem. Soc., Faraday Trans. 1 79 (1983) 2027.
[34] D. Barreca, C. Massignan, S. Daolio, M. Fabrizio, C. Piccirillo, L. Armelao, E. Tondello, Chem. Mater. 13 (2001) 588.
[35] F. Karipcin, E. Kabalcilar, S. Ilican, Y. Caglar, M. Caglar, Spectrochim. Acta Part A Mol. Biomol. Spectrosc. 73 (2009) 174.
[36] H.M. Martínez, J. Torres, L.D.L. Carreño, M.E. Rodríguez-García, Mater. Charact. 75 (2013) 184.